ADVANCED FUNCTIONAL MATERIALS

www.afm-journal.de

Distinct Bimodal Roles of Aromatic Molecules in Controlling Gold Nanorod Growth for Biosensing

Jun Hui Soh, Yiyang Lin, Michael R. Thomas, Nevena Todorova, Charalambos Kallepitis, Irene Yarovsky, Jackie Y. Ying, and Molly M. Stevens**

New aromatic molecule–seed particle interactions are examined and exploited to control and guide seed-mediated gold nanorod (Au NR) growth. This new approach enables better understanding of how small molecules impact the synthesis of metallic nanostructures, catalyzing their use in various biomedical applications, such as plasmonic biosensing. Experimental studies and theoretical molecular simulations using a library of aromatic molecules, making use of the chemical versatility of the molecules with varied spatial arrangements of electron-donating/withdrawing groups, charge, and Au-binding propensity, are performed. Au NR growth is regulated by two principal mechanisms, producing either a red or blue shift in the longitudinal localized surface plasmon resonance (LLSPR) peaks. Aromatic molecules with high redox potentials produce an increase in NR aspect ratio and red shift of LLSPR peaks. In contrast, molecules that strongly bind gold surfaces result in blue shifts, demonstrating a strong correlation between their binding energy and blue shifts produced. Through enzymatic conversion of selected molecules, 4-aminophenylphosphate to 4-aminophenol, opposing growth mechanisms at opposite extremes of target concentration are obtained, and a chemical pathway for performing plasmonic enzyme-linked immunosorbent assays is established. This unlocks new strategies for tailoring substrate design and enzymatic mechanisms for controlling plasmonic response to target molecules in biosensing applications.

1. Introduction

The emergence of novel synthetic routes towards anisotropic metallic nanoparticles (NPs) with well-controlled morphology has yielded materials with highly desirable optical and physical properties.[1] In the case of gold nanorods (Au NRs),[2] the seed-mediated growth approach has been widely studied and adopted due to the ease of control over the dispersity, size, and shape of the NRs. The resulting Au NRs exhibit longitudinal localized surface plasmon resonance (LLSPR) peaks that can be tuned across a broad spectral range (visible to near-infrared) through control of their aspect ratio. Such versatility has enabled the application of Au NRs in bioimaging,[3] optoelectronics,[4] photothermal treatment,[5] drug and gene delivery,[6] and biosensing.[7]

In a conventional seed-mediated Au NR synthesis, cetyltrimethylammonium bromide (CTAB)-stabilized gold seeds (typically 1.5–2 nm)[2c,8] are first prepared, followed by the addition of a surfactant-containing growth solution to facilitate the anisotropic growth of Au NRs. A number of parameters have been explored to tune the synthesis of Au NRs by exerting thermodynamic and kinetic controls over the growth process.[9] For example, the variation of cationic surfactants, headgroups, and their counter-ions can modify the redox potential of gold salt precursors and influence the symmetry-breaking process.[10] Control of the pH of the growth solution has been shown to modulate Au NR growth since ascorbic acid possesses a pH-dependent reduction potential.[11] The addition of aromatic and aliphatic molecules, such as salicylic acid and sodium oleate, has been found to influence the CTAB bilayer surrounding the growing NRs, improving the control over the critical symmetry-breaking event needed for anisotropic growth, and enabling the synthesis of highly monodispersed NRs with a relatively wider range of aspect ratios and dimensions.[12] A higher concentration of silver ions is understood to increase the aspect ratio of single-crystal NRs, possibly due to the underpotential deposition effect, or the formation of an $Ag[BrCTA]_2$ complex that acts as a facet-specific agent, or modification of CTAB micellization through silver–bromide interactions.[8,10,13] The reality is that the preparation of Au NRs, especially monodispersed ones, is a delicate balance of a significant number of components that affect reduction kinetics and surface free energies of growing particles, often in subtle ways that are non-obvious. Consequently, a

Dr. J. H. Soh, Dr. Y. Lin, Dr. M. R. Thomas, Dr. C. Kallepitis, Prof. M. M. Stevens
Department of Materials, Department of Bioengineering, and Institute for Biomedical Engineering
Imperial College London
Exhibition Road, London SW7 2AZ, UK
E-mail: m.stevens@imperial.ac.uk
Dr. J. H. Soh, Prof. J. Y. Ying
Institute of Bioengineering and Nanotechnology
31 Biopolis Way, The Nanos, Singapore 138669, Singapore
Dr. N. Todorova, Prof. I. Yarovsky
School of Engineering
RMIT University
Melbourne, Victoria 3001, Australia
E-mail: irene.yarovsky@rmit.edu.au

The ORCID identification number(s) for the author(s) of this article can be found under https://doi.org/10.1002/adfm.201700523.

DOI: 10.1002/adfm.201700523

more comprehensive understanding of these factors has become possible only recently.[9]

The strong absorption of light by metallic NPs makes them ideally suited for applications in biosensing, where modulation of NP aggregation or growth can lead to strong and distinct optical responses from relatively low concentrations of NPs. A popular way this phenomenon has been utilized is through the incorporation of metal NPs as part of an enzyme-linked immunosorbent assay (ELISA).[14] This leverages the high selectivity and specificity of antigen–antibody interactions, but with an added signal amplification process deriving from enzyme–substrate reactions that can be designed and harnessed to control the aggregation or overgrowth of metallic NPs. It is of particular interest to exploit the anisotropic growth of Au NRs for biosensing applications, due to their strong absorbance and the large dynamic range associated with the spectral shift in the LLSPR peaks of Au NRs (650–1200 nm), which is considerably greater than that obtainable via Au NP aggregation (520–650 nm).

This article elucidates important aromatic molecule–seed interactions that can control the anisotropic growth of Au NRs, and the resulting sensitive biosensing assays that can be developed based on modulating the plasmonic signals of Au NRs. To this end, we have examined the striking effect of a library of aromatic molecules on modulating the growth of Au NRs via two principal mechanisms. The molecules investigated could be grouped into three fundamental categories: (i) molecules acting to promote reduction, (ii) molecules acting to impede Au NR growth, as well as (iii) molecules that had no effect. We found that incubating seed particles with reducing aromatic molecules, such as 4-aminophenol (AP), led to an increase in the concentration of the seed particles. This promoted the growth of Au NRs with higher aspect ratios, which was reflected by a red shift in the LLSPR peaks. A good correlation between the spectral red shift and the redox potential (vs standard hydrogen electrode at pH 7) of the reducing molecules was established. Conversely, the addition of capping molecules, such as 4-aminophenyl phosphate (APP), blocked the surface of seed particles, and inhibited the anisotropic growth of Au NRs, resulting in a blue shift instead. Molecular dynamics (MD) simulations were employed to determine the adsorption interactions and binding affinities of the capping molecules to the Au seed surfaces and their role in modulating the Au NR growth. The same trend of Au NR growth modulation was achieved using the alkaline phosphatase (ALP)-mediated conversion of APP (a capping molecule) to AP (a reducing molecule). Au NRs with aspect ratios that ranged from 2.3 to 4.5 were obtained in an ALP concentration-dependent manner. Finally, by taking advantage of the spectral shifts derived from the physical changes of grown Au NRs, we developed a highly sensitive ELISA platform for the detection of protein biomarkers, as validated here with the detection of prostate specific antigen (PSA).

2. Results and Discussion

2.1. Bimodal Effects of Aromatic Compounds on Gold Nanorod Growth

Significant differences in the growth of Au NRs could be achieved from seeds that were incubated with subtly different aromatic compounds, differing only by a single functional group. We have discovered this to be particularly pronounced in the case of AP and APP. AP is a common reducing agent and could be generated from the dephosphorylation reaction between APP and ALP. In a typical Au NR growth reaction in our study, the seed particles were first incubated with aromatic molecules for 10 min, followed by the addition of the growth solution. Interestingly, despite having similar molecular structures, AP and APP exhibited completely opposing effects on Au NR growth; AP resulted in a red shift of the LLSPR peaks, while APP caused a blue shift (**Figure 1**a). The red shift was consistent with an increase in the aspect ratio of grown Au NRs, as seen from transmission electron microscopy (TEM) images (Figure 1b). Au NRs grown from seeds incubated with APP exhibited increased diameters and a reduced aspect ratio (2.2 for 4×10^{-5} M of APP), whereas Au NRs grown from seeds incubated with AP appeared much thinner with higher aspect ratios (4.8 for 4×10^{-5} M of AP). In addition, the aspect ratio distribution was not affected by AP/APP treatment. This phenomenon is summarized in Figure 1c. As such, we hypothesized that there were two likely effects governing the anisotropic growth of Au NRs: (i) a capping effect, where molecules bound to the seed particles and interfered with the CTAB/AgBr templated anisotropic growth,[15] and (ii) a reducing effect, where molecules acted predominantly as reducing agents.[16]

2.2. Origin of the Capping and Reducing Effects of AP and APP

The underlying mechanisms through which AP and APP influence Au NR morphology have been investigated by contrasting the effects of similarly structured aromatic molecules, including hydroquinone and 4-nitrophenyl phosphate (NPP). This allowed us to assess the need of amine functionality (capping effects) and the role of the molecules as reductants (reducing effects).

2.2.1. Reducing Effect

The mechanism through which AP was able to induce a red shift in grown Au NRs was further understood by assessing the effect of reducing molecules on seed particles. From **Figure 2**a, we observed an increase in the absorbance of the seeds after they were incubated with AP. In addition, we observed a similar dose-dependent trend between the absorbance (Abs_{515}/Abs_{700} ratio) of the seeds and the red shift obtained for grown Au NRs (Figure 2b). A similar increase in seed absorbance was also observed when seeds were incubated with a number of alternative reducing agents, such as hydroquinone, 1,4-phenylenediamine (PDA), and ascorbic acid (Figure S1a–c, Supporting Information). However, nonreducing molecules (APP and NPP) did not affect the absorbance of the seeds (Figure S1d,e, Supporting Information), confirming that an ability for reduction was required to yield a red shift in the LLSPR peaks of Au NRs.

An increase in the absorbance of Au seeds could reflect either an increase in the seed concentration or a change in size or absorbance cross-section, although the latter is usually

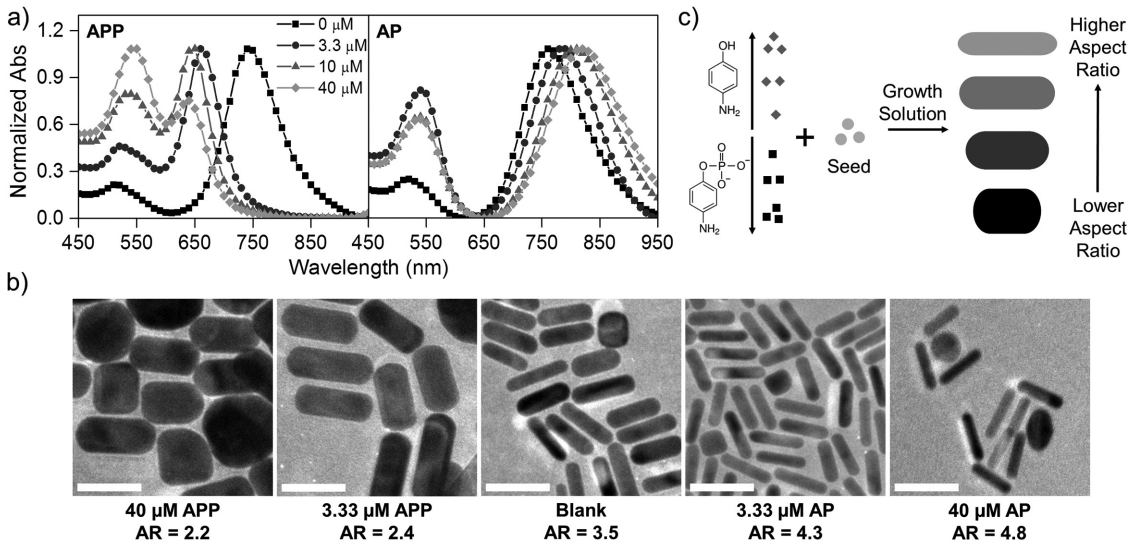

Figure 1. a) UV–vis spectra of Au NRs grown from seed particles that were incubated with various concentrations of (left) APP and (right) AP. b) TEM images of Au NRs grown from seeds that were incubated with different concentrations of APP or AP. AR = aspect ratio. Scale bars = 50 nm. c) Schematic illustrating the observed concentration-dependent effects of AP and APP on the growth of Au NRs.

coupled with a red shift in absorbance peak. To determine which parameter was responsible for generating the red shift for grown Au NRs, seeds of various concentrations and sizes were used to grow Au NRs. We found that an increase in the seed concentration resulted in a red shift in the LLSPR peaks (Figure 2c), whereas an increase in seed size led to a blue shift instead (Figure S2, Supporting Information). This suggested that incubating seeds with reducing molecules led to an increase in seed concentration. Indeed, when AP was used to reduce $HAuCl_4$ in the presence of CTAB (Figure S3, Supporting Information), a similar increase in absorbance was observed. A qualitative assessment of the seed particles by TEM (Figure S4, Supporting Information) suggested that there were no significant changes in seed size or structure observed after incubation with an increasing concentration of AP.

Furthermore, the seed-mediated growth of Au NRs tended to display a blue shift in the LLSPR peak during growth (Figure S5, Supporting Information). This was due to growth in the transverse direction,[17] after the initial burst of growth in the longitudinal direction. When the seed concentration increased, the Au^{3+} ions available for reshaping were distributed over a larger number of growing NRs. Hence, the extent of blue shift was limited. This phenomenon was observed in Figure 2d; blue shifting due to Au NR reshaping stopped after 6–10 h for higher seed concentrations, whereas blue shifting continued even after 12 h for a lower seed concentration. The same effect was observed for Au NRs grown from seed particles incubated with 3.33 and 4×10^{-5} M of AP (Figure 2e). This further suggested the ability of AP to increase the seed concentration, and consequently limit the reshaping of Au NR during growth.

The increase in seed concentration likely resulted from residual Au^{3+} ions ($[CTA]^+$–$[AuBr_4]^-$ complex) in the initial seed solution. To verify this, we attempted to completely reduce all Au^{3+} ions by increasing the concentration of $NaBH_4$ used for seed preparation. A complete Au reduction was observed using $\approx 1.4 \times 10^{-3}$ M of $NaBH_4$, as indicated by a saturation of the absorbance at 400 nm (Abs_{400}) of the seed solution (Figure S6a–b, Supporting Information). The Abs_{400} corresponded to the inter-band transition of metallic Au and could be used to monitor the reduction of Au^{3+} ions.[18] The red shift in the LLSPR peaks of grown Au NRs, as a function of AP concentration, was diminished when more $NaBH_4$ was used for seed preparation (Figure S6c, Supporting Information), highlighting the need for residual Au^{3+} in the seed solution, and the effect of initial $NaBH_4$ concentration on the extent of red shift achievable.

2.2.2. Capping Effect

In order to probe the tendency of aromatic molecules to bind to gold particles, surface-enhanced Raman spectroscopy (SERS) experiments were performed (Figure S7, Supporting Information). CTAB-stabilized seed particles were first incubated with the aromatic compounds and then grown into Au NRs. Both AP and APP displayed distinct SERS spectra as compared to Au NRs grown in the absence of any aromatic molecules (blank, Figure S7, Supporting Information). This was strongly indicative of binding since the molecules must be located close to the particle surface to generate a strong SERS signal.[19] We believe that the binding of AP and APP arose from NH_2–Au interactions. In contrast, the spectra for hydroquinone and NPP, which served as analogues of AP and APP, respectively, but without the NH_2 group, were largely similar to that of the blank, indicating a significantly weaker binding of these two molecules.

The balance between capping and reducing effects on plasmonic shifts can be highlighted by contrasting APP, AP, NPP, and hydroquinone. APP, which only demonstrated a propensity toward capping, but not a reducing effect, yielded a blue shift (Figure 1a, left), while AP, which exhibited tendencies for both

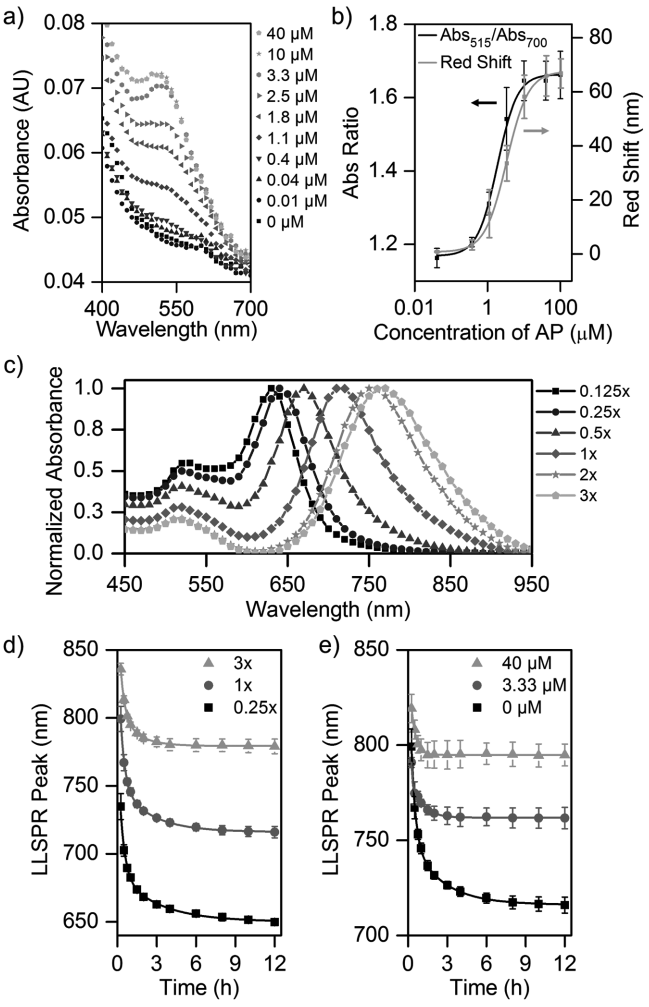

Figure 2. a) UV–vis spectra of seed particles after incubation with various concentrations of AP for 10 min. b) Comparing the changes in the absorbance of seed particles to the red shift of the LLSPR peaks obtained when those seed particles were used for NR growth. Error bars represent the standard deviation (SD), $n = 3$ independent experiments. c) UV–vis spectra of Au NRs grown from different seed concentrations, where the standard concentration described in the Experimental Section is defined as 1×. Time-evolution of the LLSPR peaks during the growth of Au NRs that were grown from d) different concentrations of seed particles, and e) seed particles that were incubated with different concentrations of AP.

capping and reduction, produced a red shift (Figure 1a, right). Hydroquinone, which demonstrated a reducing effect, but no propensity toward capping, yielded a red shift (Figure S8a, Supporting Information). As a control, NPP, which possessed neither a capping nor reducing effect, did not influence Au NR growth (Figure S8b, Supporting Information). Therefore, the results suggest that a capping effect was vital to causing a blue shift, whereas a reducing nature was key to producing a red shift in these experiments. Furthermore, for certain molecules, the reductive capacity of the molecule tended to dominate over any capping effect, as demonstrated in the case of AP. A summary of the reducing and capping effects of the molecules discussed on the LLSPR peaks of Au NRs can be found in **Table 1**.

Table 1. Summary of how the reducing and capping effects of the aromatic molecules affect the LLSPR peak of grown Au NRs.

Molecule	Reducing effect	Capping effect	Shift in LLSPR
Hydroquinone	+	–	Red shift
4-Aminophenol	+	+	Red shift
4-Aminophenyl phosphate	–	+	Blue shift
4-Nitrophenyl phosphate	–	–	No effect

Taken together, these results indicated that incubating seed particles with reducing aromatic molecules led to the nucleation of more seed particles from residual Au^{3+} ions in the seed solution. This resulted in a larger number of growing Au NRs, which in turn limited the extent of Au NR reshaping during the growth process as the ratio of Au^{3+} ions to Au NRs decreased. Consequently, Au NRs of higher aspect ratios were grown, indicated by a red shift in the LLSPR peaks, as compared to Au NRs grown without the addition of reducing molecules. In contrast, capping aromatic molecules bound to seed particles inhibited anisotropic NR growth and resulted in the production of Au NRs with lower aspect ratios.

2.3. Modulation of Gold Nanorod Growth Using a Library of Aromatic Molecules

To further probe the effects of molecular structure and chemical properties, such as functional groups, charge and binding affinity on Au NR growth, we conducted a more extensive study of Au NR growth using a library of molecules (**Figure 3**). Molecules **1**–**5** were associated with the AP family, and generally caused a red shift in the LLSPR peaks of grown Au NRs due to their reducing properties. **1** has a lower redox potential than **2**,[20] and elicited a greater red shift as it was a stronger reductant. The presence of a strong electron-donating secondary amine group for **3** resulted in an increased red shift, whereas a strong electron-withdrawing carboxyl group for **4** led to a significant decrease in the red shift. However, when the carboxyl group was not directly bonded to the benzene ring, the decrease in red shift was reduced, as observed for **5**. Furthermore, when the strong electron-donating amine group was replaced with an electron-withdrawing nitro group for **6**, there was negligible effect on Au NR growth as **6** was likely a nonreducing molecule.

The next set of molecules, **7**–**10**, was associated with the dihydroxybenzene family, and generally yielded a red shift due to their reducing effect. As **7** has a lower redox potential than **8**,[20b,21] there was a greater red shift for **7**. The presence of an electron-donating methyl group for **9** led to an increase in the red shift. Similar to the pair of **2** and **5**, the presence of a carboxyl-containing alkyl chain resulted in a decrease in the red shift for **10** as compared to **8**. When one of the electron-donating hydroxyl groups was replaced with electron-withdrawing bromide and carboxyl groups in the case of **11**, there was no effect on the growth of Au NR as **11** was likely a very weak reducing molecule.

The set of molecules, **12**–**19**, illustrated how molecular charge, negative charge in particular, and the associated pK_a of

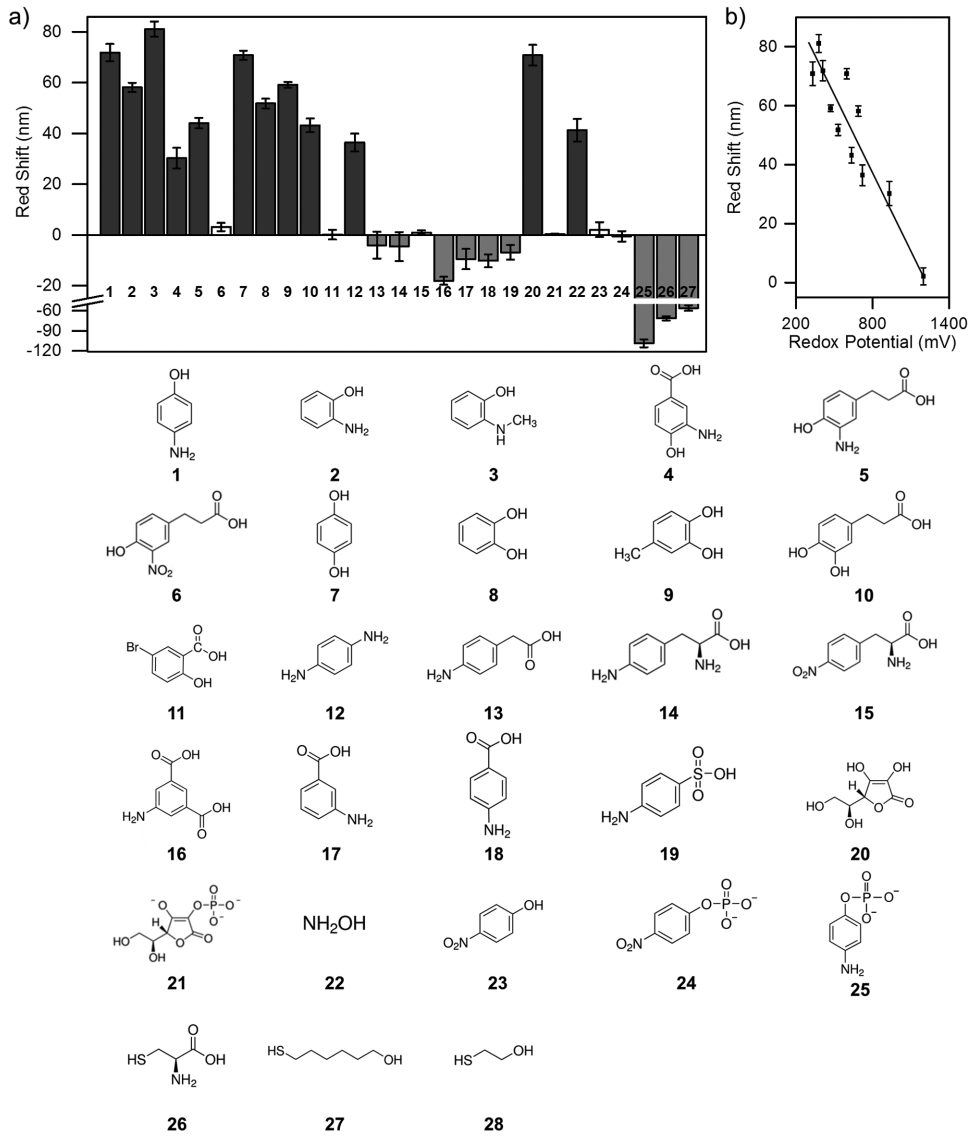

Figure 3. a) LLSPR peak shifts of Au NRs obtained when seed particles were incubated with 4×10^{-5} M of molecules **1**–**25** and 2×10^{-7} M of **26** and **27**. Negative values represent a blue shift. b) Relationship between the redox potential (vs standard hydrogen electrode at pH 7) of reducing molecules and the red shifts obtained.[20,22] (Bottom) Structures of molecules **1**–**28** investigated.

functional groups, regulated the capping effect. **12** is a common reducing agent, and thus produced a red shift. When one amine group was replaced by a carboxyl-containing alkyl chain for **13** and **14**, the molecules had no reducing effect, and were now able to cause a blue shift through capping of the seed particles via NH_2–Au interaction. When the aromatic amine group in **14** was replaced with a nitro group for **15**, there was virtually no effect on Au NR growth since **15** had neither capping nor reducing capability. The blue shifts obtained for **13** and **14** were less than that for **16**; this could be due to **16** being more negatively charged since it possesses two carboxyl groups. The negative charge was expected to help molecules bind to CTAB-capped Au seeds via electrostatic attraction. It was therefore reasonable that **25** produced a large blue shift since the phosphate group, with pK_{a1} of 2.2–3 and pK_{a2} of 6, could dissociate into a dianion under the reaction conditions. The charge effect on the extent of blue shifting was further demonstrated with **17** and **18**, which produced smaller blue shifts as compared to **16**, since the number of carboxyl group on **17** and **18** was less than that of **16**. In addition, for **19**, although the pK_a of sulfonic acids is typically <1, which is much lower than that of phosphates, there is only one deprotonating hydroxyl group for **19**, whereas there are two for **25**, causing the negative charge density of **19** to be lower than that of **25**. Therefore, a lower extent of blue shift was observed for **19** as compared to **25**.

20 and **22** are common reducing agents, and resulted in a red shift. When a phosphate group was added to **20** to yield **21**, the reducing property of **20** was deactivated, and **21** did not produce any effect on NR growth. It should be noted that **21** can also be converted to **20** enzymatically using ALP. On the other hand, **23** and **24** were ineffective in the modulation of NR growth since they possessed neither capping nor reducing effect.

The mercapto group (SH) is known as a stronger capping group, binding more readily to Au surfaces as compared to NH_2, due to covalent-like[23] thiol–Au interactions. As a result, a large blue shift (≈80 nm) was observed for **26**, even at a very low concentration of 2×10^{-7} M. In addition, we observed that **27** elicited a smaller blue shift as compared to **26**, although both contained SH groups. This could be affected by the chain length of the alkyl-thiol compound, where a shorter chain length exerts a greater inhibition of Au NR growth. This was corroborated by the observation that **28**, which has a shorter chain length as compared to **27**, virtually inhibited Au NR growth, producing mostly Au NPs (Figure S9, Supporting Information).

In agreement with our earlier discussion, we observed an inverse linear relationship between the redox potential of molecules (Table S1, Supporting Information) and the red shift obtained (Figure 3b); at a lower redox potential, the reducing strength of a molecule was greater, resulting in a larger red shift. The presence of electron-donating groups increased the reducing strength of the molecule and consequently the red shift obtained, whereas the presence of electron-withdrawing groups reduced the red shift. The substitution position of the electron-donating/withdrawing groups also influenced the red shift obtained. On the other hand, the amount of blue shift produced, was dependent on the type of Au-binding group (i.e., SH or NH_2), as well as the negative charge (pK_a-dependent) possessed by the molecule.

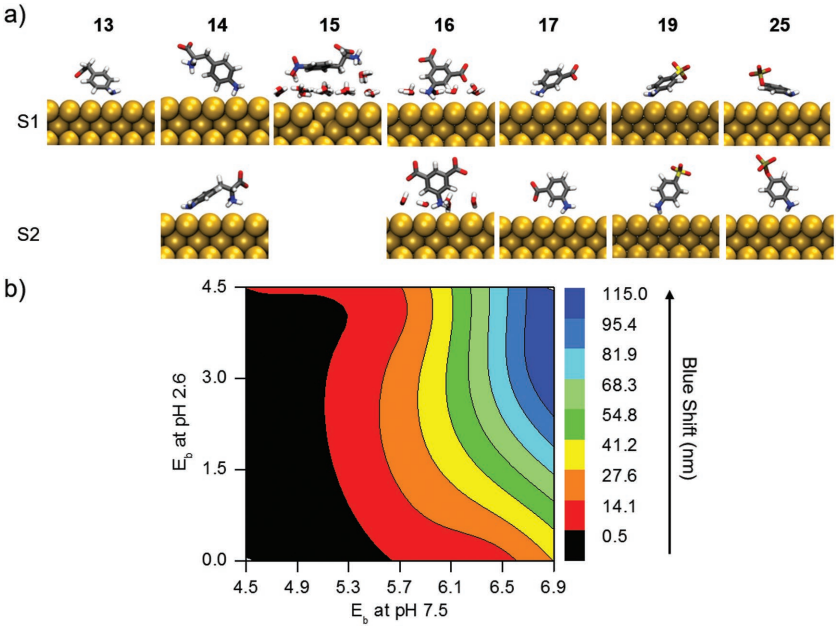

Figure 4. a) Representative structures of the most favorable binding state for each molecule and its respective binding free energies highlighted in bold in Table S2 (Supporting Information). The coordination of water molecules around the carboxylate groups is shown for molecule **16** only and omitted for the others for clarity. The color codes for the elemental composition of the structures is as follows: P and Au-yellow, C-grey, O-red, N-blue, H-white. b) Contour heat map demonstrating how theoretically calculated values of E_b at pH 2.6 and 7.5 (values taken from Table S2, Supporting Information) affected the extent of blue shift obtained experimentally. As E_b at both pH increased (toward top right region of the heat map), the amount of blue shift obtained experimentally increased as well.

The mechanisms of the adsorption interaction and binding affinities to Au were determined using theoretical molecular simulations for selected molecules (**13**, **14**, **15**, **16**, **17**, **19**, and **25**), which exhibited a tendency to promote a blue shift (**Figure 4**). The umbrella sampling method was used to determine the free energies of binding of the aromatic molecules to the dominant Au(100) surface in solution during the incubation (pH 7.5) and growth (pH 2.6) stages of Au NRs. 1D potential of mean force curves were obtained for each molecule (data not shown), from which we determined the initial association free energy (E_a), binding free energy to the Au surface (E_b), and the energy barriers ($\Delta E_{ab}/\Delta E_{bb}$) shown in Table S2 (Supporting Information).

The umbrella sampling results indicated that at pH 7.5 all molecules except **15**, exhibited spontaneous adsorption (with no free energy barrier) and bound to the surface via their amine groups in either one or two adsorption states (S1 or S2), separated by a small (thermal) barrier (Figure 4). Molecule **15**, which had the amine replaced by a nitro group (as compared to **14**), exhibited the weakest binding by adsorbing to the water monolayer, and not directly to the Au surface (Figure 4a). This phenomenon could provide a plausible explanation as to why **15** had no effect on the Au NR growth (Figure 3a). Molecule **25** exhibited the strongest binding among the molecules modeled, and presented two energetically favorable binding states (Figure 4a). The preferential orientation showed the largest contact with the Au surface, with the amine group directly on top of an Au surface atom and the center of the benzene ring commensurate with the hollow site, while the phosphate group was exposed to the solvent. The negative charge on its phosphate group could also facilitate the permeation of **25** through the CTAB layer via electrostatic interactions, which in turn could enable the free diffusion of Au ions toward the Au(100) surface[24] and restrict the anisotropic growth governed by the close binding of CTAB to the Au(100) facet.[25] These factors provide a possible explanation for the large blue shift in the LLSPR peaks of grown Au NRs with **25** as a capping agent (Figure 3a). Although the umbrella sampling results for **13**, **14**, **16**, **17**, and **19** did not directly reflect the trends observed experimentally, however, considering the two possible binding states observed for **14**, **16**, **17**, and **19** in particular, and errors associated with their free energies, the differences in their binding energetics are almost indistinguishable.

The simulations also revealed that the preferred adsorption mechanism for the aromatic molecules on Au(100) involved primary binding via NH_2–Au interaction, with the carboxylate groups in **13**, **14**, **16**, and **17**, and sulfonate group in **19** interacting with the solvent. The latter helped stabilize the adsorption of molecules to the surface via hydrogen bonding with the strongly bound water monolayer (Figure 4a). This water binding effect is due to the geometric (square) arrangement of

Au atoms on Au(100) surface, which has been shown to enable a more significant structuring of water compared to Au(111) surfaces.[26]

At pH 2.6, all molecules exhibited a weak initial adsorption to the water monolayer on the Au(100) surface, with a significantly higher energy barrier for transfer to the bare surface bound state (Table S2, Supporting Information). Overall, the amount of blue shift obtained was most likely affected by the binding of molecules during both the incubation (pH 7.5) and growth (pH 2.6) stages. Figure 4b shows how E_b at pH 2.6 and 7.5 affected the final blue shift obtained; as E_b at both pH increased, the amount of blue shift also increased. As such, the theoretical calculations identified a direct correlation between the binding affinity of the aromatic capping agents to the dominant lateral Au(100) facet[27] and their ability to modulate the anisotropic growth of Au NRs.

2.4. Modulation of Nanorod Growth via Enzymatic Dephosphorylation

The conversion of APP to AP could be easily performed via ALP-mediated dephosphorylation of APP. Utilizing this approach afforded a robust and unique route toward modulating Au NR growth through the depletion of APP and generation of AP. Prior to APP dephosphorylation, a maximal blue shift occurred, while at maximal dephosphorylation, the generation of primarily AP would elicit a strong red shift, as highlighted in **Figure 5**a. To evaluate how the growth of Au NRs could be modulated by the ALP–APP reaction, and to test its feasibility in a biosensing assay, APP was incubated with an increasing concentration of ALP to generate an increasing amount of AP. Indeed, a prominent red shift in the LLSPR peaks of the resulting Au NRs was obtained with an increasing concentration of ALP (Figure 5b). In addition, we observed a dose-dependent increase in aspect ratio (Figure 5c), which could be seen clearly by TEM (Figure 5d).

The use of the ALP–APP reaction for the modulation of Au NR growth was further applied to a sandwich ELISA (Figure S10a, Supporting Information) for the detection of the protein PSA, in order to demonstrate its feasibility in a biosensing assay. In the ELISA, an increasing concentration of PSA would lead to an increased generation of AP, resulting in the growth of Au NRs with a higher aspect ratio. This variation in aspect ratio could be readily monitored by measuring the red shift in the LLSPR peaks of grown Au NRs (Figure S10b,c, Supporting Information) for the detection of PSA. It should be noted that as NR growth is sensitive to the presence of reducing molecules such as ascorbic acid or glutathione[28] that are present in blood or serum samples, they could be potential sources of interference. However, through the stringent washing steps involved in the ELISA assay, the presence of such interfering components would be made negligible prior to the Au NR growth step and their effects kept to a minimum. The limit of detection obtained from the calibration curve (Figure S10c, Supporting Information) was 0.16 ng mL^{-1}. Since the normal physiological maximum of PSA levels for men ranges from 2.4 to 6.9 ng mL^{-1},[29] the ELISA developed is more than capable of detecting any increase in PSA levels associated with prostate cancer; demonstrating the applicability of our assay for the sensitive detection and quantification of biomarkers in biosensing and diagnostic applications.

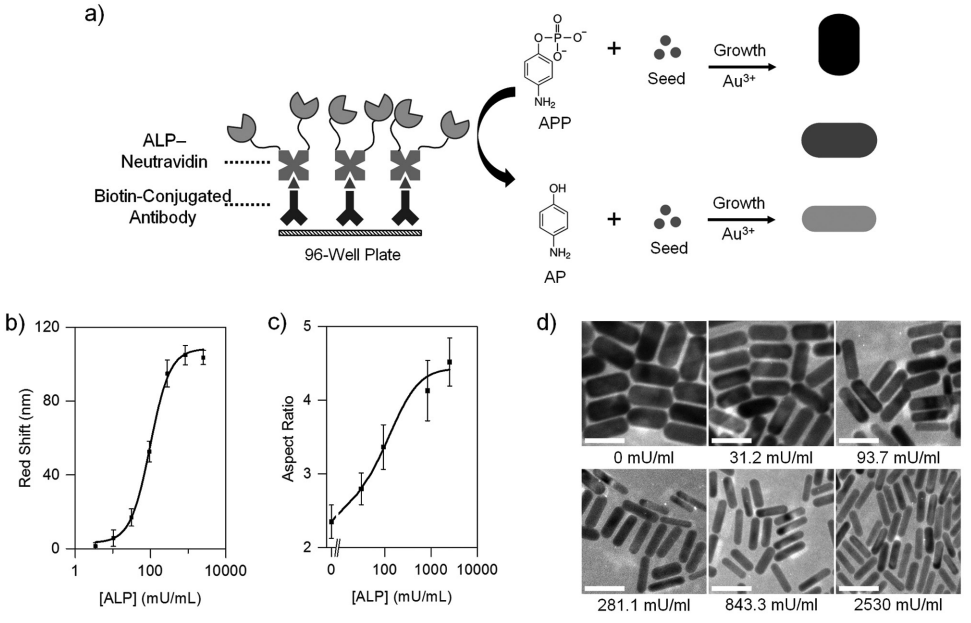

Figure 5. a) Schematic illustrating the use of ALP–APP dephosphorylation for the modulation of Au NR growth, where APP (10×10^{-6} M) was added to wells containing an increasing concentration of immobilized ALP. As the concentration of AP generated increases, Au NRs with higher aspect ratios, accompanied by a red shift of their LLSPR peaks, can be obtained. b) Red shift of the LLSPR peaks of Au NRs obtained via the ALP–APP dephosphorylation reaction. Error bars represent the SD, $n = 3$ independent experiments. c) Aspect ratios of grown Au NRs and d) their corresponding TEM images, with an increasing concentration of immobilized ALP. Scale bars = 50 nm.

3. Conclusion

We have introduced the use of aromatic reducing and capping molecules as dual effect additives for seed particles to modulate anisotropic Au NR growth. The principal mechanisms were explored and elucidated as a function of various structural and chemical processes enabling tunable Au NR growth via two potential pathways. Incubating CTAB-capped seed particles with molecules exhibiting a substantial binding affinity to the gold surface restricted the anisotropic growth of Au NRs, resulting in NRs with lower aspect ratios and a blue shift in their LLSPR peaks. Conversely, incubating the same seed particles with reducing molecules resulted in a red shift of grown Au NRs in a manner consistent with their reduction potentials. Importantly, these discrete pathways could be initiated via a single enzymatic transformation, driving a more complex reshaping process as a function of target concentration in an ELISA format. The insights gained in this work are expected to establish a more refined understanding of approaches for engineering Au NR growth through rational design of aromatic molecules, expanding the possible uses of Au NRs in diagnostic assays and many other biomedical applications.

4. Experimental Section

Materials: 4-Aminophenol (AP), 2-(methylamino)phenol, 3-amino-4-hydroxybenzoic acid, 4-nitrophenol, NPP, hydroquinone, catechol, 3,4-dihydroxyhydrocinnamic acid, PDA, 5-aminoisophtalic acid, *L*-ascorbic acid, *L*-ascorbic acid-2-phosphate, *L*-cysteine, 6-mercaptohexanol, 2-mercaptoethanol, hydroxylamine hydrochloride, gold(III) chloride hydrate ($HAuCl_4$), CTAB, silver nitrate ($AgNO_3$), hydrochloric acid solution (1.0 N), sodium borohydride ($NaBH_4$), 1-dodecanethiol, (11-mercaptoundecyl)trimethylammonium bromide, phosphate buffered saline containing 0.05% (w/v) Tween 20 (PBS–T, pH 7.4), PSA, and tissue culture treated and Nunc-Immuno MaxiSorp 96 well plates, were purchased from Sigma-Aldrich (UK). 2-aminophenol, 4-methylcatechol, and 5-bromosalicylic acid were procured from Alfa Aesar (UK). Sulfanilic acid, 3-aminobenzoic acid, and 4-aminobenzoic acid were acquired from Tokyo Chemical Industry (Japan). 4-aminophenylacetic acid, 4-amino-*L*-phenylalanine, APP, mouse monoclonal antibody against PSA (2 g L^{-1}), and biotin-modified mouse monoclonal antibody against PSA (1.2 g L^{-1}) were obtained from Abcam (UK). 4-nitro-*L*-phenylalanine was acquired from Apollo Scientific Ltd. (UK). 4-(2-hydroxyethyl)-1-piperazineethanesulfonic acid (HEPES) buffer (1 M, pH 8.0) was bought from VWR (UK). Nuclease-free water, SuperBlock (Tween 20, PBS) blocking buffer, neutravidin-modified alkaline phosphatase (neutravidin-ALP), and 1× PBS (pH 7.2) were acquired from Life Technologies (UK). Dialysis kit, with a molecular weight cut-off (MWCO) of 1 kDa, was procured from GE Healthcare (UK).

Seed-Mediated Growth of Au NRs: The seed solution was prepared by adding 500 µL of CTAB (0.2 M) to $HAuCl_4$ (500 µL, 5×10^{-4} M), followed by adding 60 µL of freshly prepared $NaBH_4$ (8.4×10^{-3} M). The seed solution (pH 4.0) was then stirred vigorously for a minute and kept at room temperature for ≈1 h before use.

The growth solution (pH 2.2) was prepared by adding 500 µL of CTAB (0.2 M) to $HAuCl_4$ (500 µL, 2×10^{-3} M), followed by the sequential addition of 20 µL of $AgNO_3$ (4×10^{-3} M), 102 µL of ascorbic acid (1.2×10^{-2} M), and 9 µL of HCl (1.0 N). The volume described here is sufficient for the growth of Au NRs in 10 wells and can be scaled up accordingly.

For the growth of Au NRs, 1 µL of the seed solution was added to 50 µL of HEPES buffer (5×10^{-3} M, pH 7.8). The mixture had a pH of 7.5. This was followed by adding 110 µL of the growth solution (final pH = 2.6). The solution was stirred after adding each component and left to incubate for overnight (16–20 h) at room temperature.

For tuning the growth of Au NRs using aromatic molecules, 1 µL of the seed solution was added to 50 µL of aromatic molecule solution (prepared in 5×10^{-3} M of HEPES buffer), and incubated for 10 min at room temperature. 110 µL of the growth solution was then added, and Au NR growth was left to incubate overnight at room temperature. Note: a stock solution of aromatic molecules (1×10^{-2} M) was first prepared in 5×10^{-3} M of HEPES buffer, and desired concentrations of aromatic molecules were prepared through serial dilution in 5×10^{-3} M of HEPES.

Supporting Information

Supporting Information is available from the Wiley Online Library or from the author.

Acknowledgements

M.M.S. thanks the Engineering and Physical Sciences Research Council (EPSRC), Grant EP/K020641/1, for funding. I.Y. and M.M.S. acknowledge the Australian Research Council for financial support under the Discovery Project scheme (DP140101888 and DP170100511). M.R.T. and M.M.S. thank the i-sense EPSRC IRC in Early Warning Sensing Systems for Infectious Diseases (EP/K031953/1), for funding. The authors thank Dr. Christopher Spicer for providing molecules **5** and **6**. This research was undertaken with the assistance of resources from the National Computational Infrastructure (NCI), grant number (e87) and Victorian Life Sciences Computation Initiative (VLSCI) grant number (VR0202), Australia. J.H.S. is grateful to the Agency for Science, Technology and Research (A*STAR), Singapore, for support and provision of the A*STAR Graduate Scholarship. All raw data are available on request from M.M.S. for experimental and I.Y. for simulations.

Conflict of Interest

The authors declare no conflict of interest.

Keywords

alkaline phosphatase, anisotropic growth, aromatic additives, gold nanorods, plasmonic sensing

Received: January 27, 2017
Revised: April 7, 2017
Published online: June 26, 2017

[1] a) C. J. Murphy, T. K. San, A. M. Gole, C. J. Orendorff, J. X. Gao, L. Gou, S. E. Hunyadi, T. Li, *J. Phys. Chem. B* **2005**, *109*, 13857; b) M. Rycenga, C. M. Cobley, J. Zeng, W. Y. Li, C. H. Moran, Q. Zhang, D. Qin, Y. N. Xia, *Chem. Rev.* **2011**, *111*, 3669; c) P. D. Howes, R. Chandrawati, M. M. Stevens, *Science* **2014**, *346*, 124739001.

[2] a) N. R. Jana, L. Gearheart, C. J. Murphy, *J. Phys. Chem. B* **2001**, *105*, 4065; b) N. R. Jana, L. Gearheart, C. J. Murphy, *Adv. Mater.* **2001**, *13*, 1389; c) B. Nikoobakht, M. A. El-Sayed, *Chem. Mater.* **2003**, *15*, 1957.

[3] X. H. Huang, I. H. El-Sayed, W. Qian, M. A. El-Sayed, *J. Am. Chem. Soc.* **2006**, *128*, 2115.

[4] P. Zijlstra, J. W. M. Chon, M. Gu, *Nature* **2009**, *459*, 410.

[5] G. von Maltzahn, A. Centrone, J. H. Park, R. Ramanathan, M. J. Sailor, T. A. Hatton, S. N. Bhatia, *Adv. Mater.* **2009**, *21*, 3175.

[6] a) A. M. Alkilany, L. B. Thompson, S. P. Boulos, P. N. Sisco, C. J. Murphy, *Adv. Drug Delivery Rev.* **2012**, *64*, 190; b) A. K. Salem, P. C. Searson, K. W. Leong, *Nat. Mater.* **2003**, *2*, 668.
[7] a) A. V. Kabashin, P. Evans, S. Pastkovsky, W. Hendren, G. A. Wurtz, R. Atkinson, R. Pollard, V. A. Podolskiy, A. V. Zayats, *Nat. Mater.* **2009**, *8*, 867; b) L. B. Wang, Y. Y. Zhu, L. G. Xu, W. Chen, H. Kuang, L. Q. Liu, A. Agarwal, C. L. Xu, N. A. Kotov, *Angew. Chem. Int. Ed.* **2010**, *49*, 5472; c) X. H. Huang, S. Neretina, M. A. El-Sayed, *Adv. Mater.* **2009**, *21*, 4880; d) J. H. Soh, Z. Gao, in *Complex-Shaped Metal Nanoparticles* (Ed: T. K. Sau, A. L. Rogach), Wiley-VCH Verlag GmbH & Co. KGaA, Weinheim, Germany, **2012**, p. 477.
[8] M. Z. Liu, P. Guyot-Sionnest, *J. Phys. Chem. B* **2005**, *109*, 22192.
[9] L. Scarabelli, A. Sánchez-Iglesias, J. Pérez-Juste, L. M. Liz-Marzán, *J. Phys. Chem. Lett.* **2015**, *6*, 4270.
[10] N. Almora-Barrios, G. Novell-Leruth, P. Whiting, L. M. Liz-Marzan, N. Lopez, *Nano Lett.* **2014**, *14*, 871.
[11] G. Gramlich, J. Zhang, W. M. Nau, *J. Am. Chem. Soc.* **2002**, *124*, 11252.
[12] a) X. C. Ye, C. Zheng, J. Chen, Y. Z. Gao, C. B. Murray, *Nano Lett.* **2013**, *13*, 765; b) X. Ye, L. Jin, H. Caglayan, J. Chen, G. Xing, C. Zheng, V. Doan-Nguyen, Y. Kang, N. Engheta, C. R. Kagan, C. B. Murray, *ACS Nano* **2012**, *6*, 2804.
[13] a) S. R. Jackson, J. R. McBride, S. J. Rosenthal, D. W. Wright, *J. Am. Chem. Soc.* **2014**, *136*, 5261; b) F. Hubert, F. Testard, O. Spalla, *Langmuir* **2008**, *24*, 9219.
[14] a) W. S. Qu, Y. Y. Liu, D. B. Liu, Z. Wang, X. Y. Jiang, *Angew. Chem. Int. Ed.* **2011**, *50*, 3442; b) J. H. Soh, Y. Y. Lin, S. Rana, J. Y. Ying, M. M. Stevens, *Anal. Chem.* **2015**, *87*, 7644; c) Z. Zhang, Z. Chen, S. Wang, F. Cheng, L. Chen, *ACS Appl. Mater. Int.* **2015**, *7*, 27639; d) Y. Li, X. Ma, Z. Xu, M. Liu, Z. Lin, B. Qiu, L. Guo, G. Chen, *Analyst* **2016**, *141*, 2970.
[15] M. Coronado-Puchau, L. Saa, M. Grzelczak, V. Pavlov, L. M. Liz-Marzan, *Nano Today* **2013**, *8*, 461.
[16] A. George, P. V. Thomas, D. D. Kumar, *Chemist* **2013**, *86*, 15.
[17] D. A. Zweifel, A. Wei, *Chem. Mater.* **2005**, *17*, 4256.
[18] L. Scarabelli, M. Grzelczak, L. M. Liz-Marzán, *Chem. Mater.* **2013**, *25*, 4232.
[19] B. Nikoobakht, M. A. El-Sayed, *J. Phys. Chem. A* **2003**, *107*, 3372.
[20] a) H. Beiginejad, D. Nematollahi, F. Varmaghani, *J. Electrochem. Soc.* **2013**, *160*, H41; b) S. Steenken, P. Neta, *J. Phys. Chem.* **1982**, *86*, 3661; c) K. Prasain, T. D. T. Nguyen, M. J. Gorman, L. M. Barrigan, Z. Y. Peng, M. R. Kanost, L. U. Syed, J. Li, K. Y. Zhu, D. H. Hua, *Bioorg. Med. Chem.* **2012**, *20*, 1679.
[21] Y. A. Ilan, G. Czapski, D. Meisel, *Biochim. Biophys. Acta* **1976**, *430*, 209.
[22] a) C. X. Chen, X. Z. Hong, Y. H. Gao, *J. Appl. Polym. Sci.* **2015**, *132*, 42190; b) C. X. Chen, G. Q. Ding, D. Zhou, X. H. Lu, *Electrochim. Acta* **2013**, *97*, 112; c) D. Nematollahi, S. M. Golabi, *J. Electroanal. Chem.* **1996**, *405*, 133; d) M. Salas-Reyes, J. Hernandez, Z. Dominguez, F. J. Gonzalez, P. D. Astudillo, R. E. Navarro, E. Martinez-Benavidez, C. Velazquez-Contreras, S. Cruz-Sanchez, *J. Braz. Chem. Soc.* **2011**, *22*, 693; e) T. Iyanagi, I. Yamazaki, K. F. Anan, *Biochim. Biophys. Acta* **1985**, *806*, 255; f) V. D. Pedrosa, L. Codognoto, L. A. Avaca, *J. Braz. Chem. Soc.* **2003**, *14*, 530.
[23] a) R. A. Sperling, W. J. Parak, *Philos. Trans. R. Soc., A* **2010**, *368*, 1333; b) Y. Xue, X. Li, H. Li, W. Zhang, *Nat. Commun.* **2014**, *5*, 4348.
[24] S. K. Meena, M. Sulpizi, *Langmuir* **2013**, *29*, 14954.
[25] J. Gao, C. M. Bender, C. J. Murphy, *Langmuir* **2003**, *19*, 9065.
[26] L. B. Wright, J. P. Palafox-Hernandez, P. M. Rodger, S. Corni, T. R. Walsh, *Chem. Sci.* **2015**, *6*, 5204.
[27] a) Z. L. Wang, M. B. Mohamed, S. Link, M. A. El-Sayed, *Surf. Sci.* **1999**, *440*, L809; b) B. Goris, S. Bals, W. Van den Broek, E. Carbo-Argibay, S. Gomez-Grana, L. M. Liz-Marzan, G. Van Tendeloo, *Nat. Mater.* **2012**, *11*, 930.
[28] a) S. A. Margolis, D. L. Duewer, *Clin. Chem.* **1996**, *42*, 1257; b) F. Michelet, R. Gueguen, P. Leroy, M. Wellman, A. Nicolas, G. Siest, *Clin. Chem.* **1995**, *41*, 1509.
[29] a) J. E. Oesterling, S. J. Jacobsen, C. G. Chute, H. A. Guess, C. J. Girman, L. A. Panser, M. M. Lieber, *JAMA* **1993**, *270*, 860; b) B. L. Dalkin, F. R. Ahmann, J. B. Kopp, *J. Urol.* **1993**, *150*, 1837; c) E. P. DeAntoni, E. D. Crawford, J. E. Oesterling, C. A. Ross, E. R. Berger, D. G. McLeod, F. Staggers, N. N. Stone, *Urology* **1996**, *48*, 234.